EVALUATING SPOT WELDS OF DISSIMILAR METALS VIA INTEGRATED MECHANICAL TESTING AND FINITE ELEMENT MODELING

UDC:621.791.763
Original scientific paper https://doi.org/10.46793/aeletters.2025.10.2.2

Kamal Abdulkareem Mohammed[1], Ahmed Ali Farhan Ogaili[*1], Abdul Wahab A. Taha[1], Ahmed Mohsin Alsayah[2]

[1]Mechanical Engineering Department, College of Engineering, Mustansiriyah University, Baghdad 10052, Iraq
[2]Refrigeration & Air-condition Department, Technical Engineering College, The Islamic University, Najaf, Iraq

Abstract:
This study investigates resistance spot welding of dissimilar materials, namely 37.2 carbon steel, 304 stainless steel, and commercial aluminium. The effect of welding parameters on nugget growth, tensile shear strength, and failure modes in various material combinations was investigated using a combined experimental and finite element modeling (FEM) approach. Experimental studies included a welding current range (5-15 kA) and time range (10-30 cycles), complemented by tensile testing and hardness measurements. It was observed that Carbon Steel-Stainless Steel (CS-SS) joints achieved the highest strength (9.5 kN at 9 kA), while aluminium-containing joints exhibited lower strengths but required higher optimal currents. Hardness profiles showed extensive variations across weld zones, particularly for aluminium-steel joints. Failure mode analysis showed a prevalence of pullout failures for CS-SS joints, in contrast to more interfacial failures in aluminium-steel combinations. A finite element model was developed and validated against experimental data, showing excellent predictive capability for nugget size and joint strength ($R^2 > 0.96$). This study contributes to the development of dissimilar material welding by providing new insights into parameter optimization, failure mechanisms, and industrial application, particularly for automotive and aerospace industries.

ARTICLE HISTORY
Received: 10 February 2025
Revised: 1 March 2025
Accepted: 18 March 2025
Published: 30 June 2025

KEYWORDS
Dissimilar Metals, Tensile shear strength, Failure modes, Finite element analysis, Welding parameters

1. INTRODUCTION

The growing demand for lightweight, multi-material bodies in automotive and aerospace applications has intensified the need for reliable joining of dissimilar metals [1]. Resistance spot welding (RSW), renowned for its speed and amenability to automation, faces significant hurdles when joining material pairs with dissimilar thermo-mechanical properties, e.g., carbon steel (CS), stainless steel (SS), and aluminium (Al) [2]. While past studies have considered RSW of individual dissimilar pairs (e.g., Al-steel or CS-SS), significant gaps exist in the understanding of the interplay of welding parameters, interfacial reactions, and failure mechanisms for tri-material systems—a configuration of increasing significance in modern lightweight designs [3]. Through a study of the response of these materials to spot welding, this project aims to develop optimized welding procedures that enhance the strength and reliability of multilateral bodies. Tensile testing and finite element modeling (FEM) are used in the investigation to evaluate weld quality, predict failure locations, and develop insight into the complex interplay between welding parameters and joint characteristics.

*CONTACT: Ahmed Ali Farhan Ogaili, e-mail: ahmed_ogaili@uomustansiriyah.edu.iq

2. LITERATURE REVIEW

Resistance spot welding (RSW) of dissimilar materials has gained significant attention due to its critical role in modern manufacturing, particularly for lightweight multi-material structures in automotive and aerospace applications.

Some researchers focus on the challenges of dissimilar material welding, such as Yang et al. [3] conducted an extensive review of RSW for dissimilar materials, emphasizing the challenges posed by differences in thermal and electrical properties. The importance of optimizing welding parameters to achieve strong and reliable joints was highlighted. In the context of automotive applications, Łomozik et al. [4] investigated the failure mechanisms of dissimilar spot welds between low-carbon steel and austenitic stainless steel, focusing on the microstructure and mechanical properties of the weld nugget as critical factors for joint performance. Advancements in experimental techniques have provided deeper insights into dissimilar material welding. For instance, Dong et al. [5] utilized digital image correlation to analyse local deformation in dissimilar resistance spot welds under tensile-shear loading, revealing valuable information about strain distribution around the weld nugget. Additionally, Mehta et al. [6] reviewed friction stirspot welding as an alternative to traditional RSW, demonstrating its potential for joining challenging material combinations.

Another issue with aluminium-steel Joints studies, such as the welding of aluminium to steel, remains a significant challenge due to its importance in lightweight vehicle design. Winnicki et al. [7] studied the microstructure and mechanical properties of resistance spot welds between aluminium alloy and zinc-coated steel, while Mori et al. [8] explored magnetic pulse welding as an alternative technique for joining ultra-high-strength steel and aluminium alloy.

Fatigue behaviour of dissimilar spot welds between steel and aluminium alloys was investigated by Shi et al. [9], providing insights into their long-term performance**.**

Recent developments in non-destructive testing have significantly improved the evaluation of spot welds. Liu et al. [10] conducted an extensive study on ultrasonic testing, demonstrating its efficiency in detecting internal defects and estimating nugget size. Verma et al. [11] combined FEA with experimental ultrasonic testing to analyse wave propagation in welded joints of varying compositions, emphasizing the impact of material heterogeneity on numerical simulations. Pouranvari [12] examined the relationship between microstructure and mechanical performance in dissimilar resistance spot welds, focusing on the role of martensite formation in the fusion zone.

Significant progress has been made in modeling spot welds using finite element analysis (FEA). Kong et al. [13] developed a three-dimensional FEM model to simulate temperature distribution and nugget formation during RSW of dissimilar aluminium alloys. Similarly, Adkine and Biradar [14] investigated the strength and failure characteristics of aluminium-steel spot welds using experimental and numerical methods, highlighting the complexity introduced by interfacial reactions. Russo Spena et al. [15] studied the mechanical behaviour of dissimilar spot welds between advanced high-strength steel and aluminium alloys, identifying nugget size and chemical composition as critical factors influencing joint strength. In Table 1, a summary of the methodologies used in spot welding research is presented.

Table 1. Employed methodologies in spot welding research for both similar and dissimilar materials

Methodology	Description	Key References
Experimental Tensile Testing	Evaluates mechanical strength and failure modes of welded joints	Pouranvari and Marashi [16]
Microstructural Analysis	Examines weld nugget composition and interfacial reactions	Wan et al. [17]
Finite Element Modeling	Simulates welding process and predicts joint behaviour	Kong et al. [13]
Process Parameter Optimization	Investigates the effects of welding current, time, and force	Zhang et al. [18]
Digital Image Correlation	Analyses local deformation behaviour during testing	Dong et al. [5]
Fatigue Testing	Assesses long-term performance under cyclic loading	Khanna and Long [19]
Alternative Welding Techniques	Explores novel joining methods for challenging material combinations	Mori et al. [8]
Machine Learning Approaches	Utilizes data-driven methods to optimize welding parameters	Bogaerts et al. [20]

Despite substantial contributions from previous studies, several aspects remain unexplored. These include comprehensive investigations of tri-

material systems, systematic parameter optimization for dissimilar material combinations, and detailed failure mode analyses under complex loading conditions. This study aims to address these gaps by focusing on the following areas:

- Comprehensive material combination: A detailed investigation of 37.2 carbon steel, 304 stainless steel, and commercial aluminium.
- Integrated experimental-numerical approach: Combining tensile testing with finite element modeling to predict joint behaviour under complex loading conditions.
- Systematic parameter study: Evaluating the interaction of welding parameters with joint quality across material combinations.
- Failure mode analysis: Providing a complete understanding of failure mechanisms in dissimilar material resistance spot welds.
- Industrial utilization: Offering practical insights for automotive and aerospace manufacturing industries.

This study contributes to advancing the understanding of dissimilar material spot welding, bridging the gap between theoretical knowledge and industrial implementation.

3. MATERIAL AND METHODS

This section delineates the methodological approach employed to investigate the resistance spot welding of dissimilar materials, specifically AISI 304 stainless steel, 37.2 carbon steel, and commercial aluminium. The methodology encompasses material characterization, welding process optimization, and post-weld analysis techniques.

3.1 Materials and Specimen Preparation

Three materials were selected for this study due to their widespread industrial applications and disparate thermo-mechanical properties: AISI 304 stainless steel, 37.2 carbon steel, and commercial aluminium. These materials represent a range of properties commonly encountered in dissimilar material joining applications, particularly in the automotive and aerospace industries. The thermophysical and electrical properties of the materials being used for the purpose of resistance spot welding (RSW) strongly impact heat formation, heat loss, and weld formation. Of note is the high value for the thermal conductivity for commercial aluminium being 237 W/m·K, some 14.6 times the value for the 304 stainless steel being 16.2 W/m·K. This high value produces non-uniform heat loss patterns during welding processes, and welding parameters must be carefully controlled for counteraction against the high heat conducting capability of aluminium, resulting in inhibition of nugget formation when compared against steel-dominated welds [21]. Moreover, variations in the resistivity make the welding dynamics even more complicated. For instance, the low value for the resistivity for carbon steel is 0.16 μΩ·m, which allows for localized build-up of the heat by Joules at steel–aluminium interfaces. Aluminium has much less resistivity, about 0.028 μΩ·m, and the welding process thus requires larger currents (between 8–9 kA) for the desired heat input [22]. These materials also differ by their melting points; aluminium has one around about 660°C, while steel has one from 1400–1530°C. This also has implications for the kinetics of the interfacial reaction, where the lower aluminium melting temperature favours preferential aluminium melting and the formation of intermetallic compounds (IMCs) at the weld interface. These mismatches in the materials' properties reflect the inherent limitations for welding the dissimilar metals and the necessity for optimizing welding parameters for the sound weld formation [23]. Table 2 presents the salient properties of these materials, determined through standardized testing procedures

Table 2. Material Properties of AISI 304 Stainless Steel, 37.2 Carbon Steel, and Commercial Aluminium [24, 25]

Property	AISI 304 Stainless Steel	37.2 Carbon Steel	Commercial Aluminium
Yield Strength (MPa)	215 ± 4	250 ± 5	110 ± 3
Ultimate Tensile Strength (MPa)	505 ± 10	450 ± 8	180 ± 5
Elastic Modulus (GPa)	193 ± 3	200 ± 4	70 ± 2
Poisson's Ratio	0.29 ± 0.01	0.30 ± 0.01	0.33 ± 0.01
Density (kg/m³)	8000 ± 20	7850 ± 15	2700 ± 10
Thermal Conductivity (W/m·K)	16.2 ± 0.2	51.9 ± 0.5	237 ± 5
Specific Heat Capacity (J/kg·K)	500 ± 5	486 ± 5	897 ± 10
Electrical Resistivity (μΩ·m)	0.72 ± 0.01	0.16 ± 0.005	0.0282 ± 0.0005
Coefficient of Thermal Expansion (10^{-6}/K)	17.3 ± 0.3	11.7 ± 0.2	23.1 ± 0.5
Melting Point Range (°C)	1400-1450	1470-1530	660-670

3.2 Specimen Preparation

Specimens were prepared in accordance with AWS D8.9M:2012 standards. Sheets of AISI 304 stainless steel, 37.2 carbon steel, and commercial aluminium were precision-cut into 25 mm x 100 mm specimens with a thickness of 1 ± 0.2 mm using a computer numerical control (CNC) laser cutting machine as shown in Fig. 1. A total of 180 specimens were prepared, comprising 60 specimens each of stainless steel, carbon steel, and aluminium. Surface preparation followed a rigorous protocol to ensure consistent surface conditions across all specimens:

- Degreasing in an acetone bath for 5 minutes
- Mechanical cleaning using a stainless-steel wire brush (20 passes in alternating directions).
- Sequential polishing with 220, 400, and 600 grit sandpaper (50 strokes in each direction for each grit size).
- Ultrasonic cleaning in ethanol for 10 minutes followed by drying with a lint-free cloth in a laminar flow hood.

This meticulous preparation process ensured uniform surface conditions, which are critical for achieving consistent weld quality across all specimens. Fig. 1 illustrates the specimen dimensions and the overlap configuration used for the welding process.

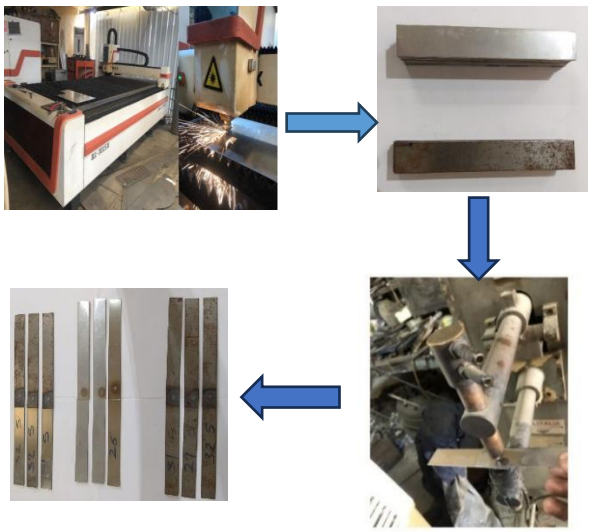

Fig. 1. The procedures for preparing the samples

The wide range of material properties, particularly the differences in thermal and electrical conductivity, melting points, and strength, presents significant challenges in achieving high-quality welds across these dissimilar material combinations. These differences form the basis for the comprehensive investigation of welding parameters and their effects on weld quality and joint strength in the subsequent sections of this study.

3.3. Welding Process

Resistance spot welding was performed using a Nabertherm RSW 100 Medium Frequency Direct Current (MFDC) spot welding machine. This equipment was selected for its precise control over welding parameters and its suitability for joining dissimilar materials. The machine was calibrated before each welding session using a Miyachi MM-122A current meter and a Tecna TE1600 force gauge to ensure accuracy and repeatability of the welding parameters. The following welding parameters were systematically varied to investigate their effects on weld quality:

- Welding Current: 5-15 kA (1 kA increments).
- Welding Time: 10-30 cycles (5 cycle increments, based on 60 Hz power supply).
- Electrode Force: 2-6 kN (0.5 kN increments).
- Hold Time: 5-15 cycles (2 cycle increments).
- Electrode Tip Diameter: 6, 7, and 8 mm.

The electrode tip diameter was calculated using the following equation, which is generally applicable for low carbon steel:

Electrode tip diameter = 0.100" + 2t.

Where "*t*" is the thickness (in inches) of one thickness of the welded metal. A full factorial experimental design was implemented to thoroughly explore the parameter space. For each material combination (CS-SS, CS-Al, SS-Al), 20 specimens were prepared, resulting in a total of 60 welded specimens. The welding sequence was randomized to minimize systematic errors.

3.4. Mechanical Testing

3.4.1 Tensile Testing

Tensile-shear tests were conducted using an Instron 5985 Universal Testing Machine equipped with a 250 kN load cell, in accordance with AWS D8.9M:2012 standard as shown in Fig. 2. The following test parameters were used:

- Crosshead speed: 10 mm/min.
- Data acquisition rate: 100 Hz.
- Temperature: Room temperature (23 ± 2°C).
- Humidity: 50 ± 5% RH.

A National Instruments cDAQ-9178 data acquisition system was used to record load and displacement data [26].

Fig. 2. Tensile Test

3.4.2 Hardness Testing

Vickers microhardness measurements were taken using a Buehler MicroMet 6040 microhardness tester used in this study as shown in Fig. 3. The testing parameters were as follows:

- Applied load: 100 gf.
- Dwell time: 10 seconds.
- Indentation spacing: 0.1 mm intervals across the weld cross-section.

Fifteen indentations were made across each material sample in a 3x5 grid pattern with 5 mm spacing between indentations to create a comprehensive hardness map of the weld and surrounding areas.

Fig. 3. Hardness Test

3.5 Finite Element Analysis

Finite element analysis (FEA) is a computational method widely used in engineering to simulate and analyse complex systems, providing detailed insights into physical phenomena that are difficult to observe experimentally [27–29]. In this study, FEA was employed to model the resistance spot welding process and predict the mechanical behaviour of the welded joints. The analysis was conducted using Abaqus/Explicit 2017, a state-of-the-art software suite known for its robust capabilities in handling dynamic and nonlinear problems [30].

3.5.1 Model Geometry and Mesh

The geometric configuration of the resistance spot welding model was developed with exceptional precision to ensure accurate representation of the physical welding process. Fig. 4 shows the model building upon the foundational work of [31], who established critical dimensional parameters for multi-material welding simulations. The model incorporated detailed specifications for each component. The electrode geometry followed the Type-B configuration specified in ISO 5821, featuring a truncated cone design with a 16 mm body diameter tapering to a 6mm face diameter. The electrode tip exhibited a 40mm radius of curvature, which in paper demonstrated as optimal for preventing excessive edge wear while maintaining current density distribution. The total electrode length was maintained at 25 mm to accurately capture heat dissipation effects. The workpiece assembly consisted of three distinct layers, each with dimensions of 120 mm length, 1 mm thickness, and 25 mm width, following the EN ISO 14329 standard. The layers included: A 1.0 mm thick 37.2 carbon steel sheet, and a 1.5 mm thick 304 stainless steel intermediate layer, a 2.0 mm thick commercial aluminium sheet

The overlap region between the sheets was set to 25 mm, ensuring sufficient contact area for weld nugget formation. The overall model dimensions were carefully selected to minimize boundary effects while maintaining computational efficiency, as recommended by [32].

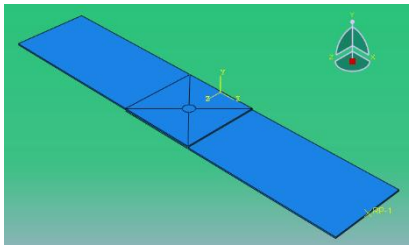

Fig. 4. Model Geometry

This dimensional configuration provided sufficient distance from the weld centre to the

model boundaries, enabling accurate representation of thermal gradients and mechanical constraints.

3.5.2 Material Properties and Constitutive Models

It was performed to simulate the complex. Temperature-dependent material properties were implemented for all three materials. The Johnson-Cook plasticity model was utilized to account for the complex behaviour of materials during the welding process. The model parameters were calibrated using experimental data from high-temperature tensile tests.

3.5.3 Boundary Conditions and Loading

A fully coupled thermal-electrical-mechanical analysis of interactions during the welding process. The welding cycle was simulated in three distinct steps:

1. Squeeze step: Application of electrode force.
2. Weld step: Application of current and heat generation.
3. Hold step: Cooling under maintained electrode force.

Thermal and electrical contact conditions between the electrodes and workpieces were defined using surface-to-surface contact pairs with temperature-dependent properties.

3.5.4 Meshing Strategy

The workpiece was meshed using 3D linear hexahedral elements of type C3D8R, widely employed in finite element analysis (FEA) for their ability to capture complex geometries and structural behaviour in thermal and mechanical simulations. A multi-scale meshing strategy was implemented:

- **Weld Nugget and HAZ Regions**: Element sizes refined to 0.05–0.1 mm to resolve steep thermal gradients and localized material behaviour.
- **Far-Field Regions**: Element sizes gradually increased to 1 mm in areas distant from the weld zone, reducing computational cost without compromising accuracy.

The final mesh consisted of approximately 22,360 elements, combining hexahedral and tetrahedral elements to accommodate complex geometries and ensure smooth transitions as shown in Fig 5. Hexahedral elements were predominantly used in the weld nugget and heat-affected zone (HAZ) for superior stress and thermal analysis performance. In contrast, tetrahedral elements were employed in irregular geometries to maintain mesh quality.

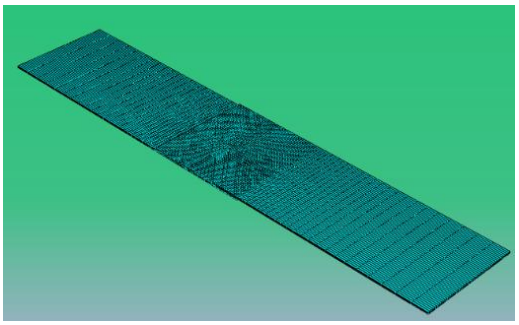

Fig. 5. Mesh coverage

3.5.5 Mesh Sensitivity Analysis

A comprehensive mesh convergence study was conducted to determine the optimal balance between computational accuracy and efficiency . The analysis evaluated the impact of global mesh refinement on the maximum von Mises stress, as shown in Fig. 6. Results demonstrate that stress values stabilize at 22,360 elements, with further refinement to 50,495 elements yielding only a 1.8% increase in stress (621 MPa vs. 610 MPa). This confirms mesh independence beyond 21,160 elements, validating the selected mesh configuration.

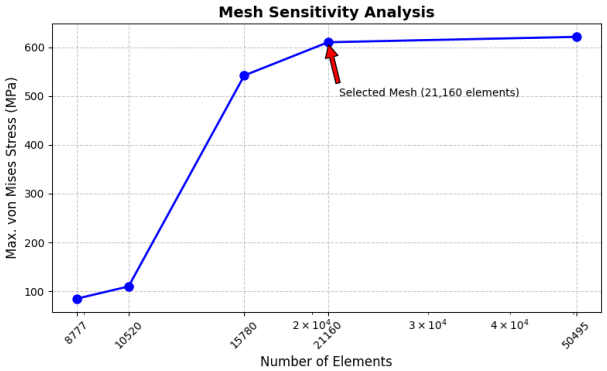

Fig. 6. Mesh Sensitivity Analysis of RSW Joints

Key findings align with Chigurupati et al. [33], who emphasized that coarse meshes underestimate critical stresses, while over-refined meshes incur unnecessary computational costs. The final model employs 21,160 elements (25,784 nodes) with zonal refinement, Weld Nugget: 0.05 mm elements (45,000 elements) HAZ: 0.05–0.15 mm graded elements (65,000 elements), Far-Field: 1 mm elements (40,000 elements).

This configuration achieved <1% variation in nugget diameter predictions during validation, satisfying the convergence criteria of the study [34].

3.5.6 Simulation Output and Validation

The following key results were extracted from the FEA simulations: Temperature distribution and thermal history, Stress and strain fields, Predicted weld nugget size and shape. These simulation results were validated against experimental data, including nugget dimensions and tensile-shear test results. Fig. 7. illustrate the Von mises stress of the RWS of CS-SS.

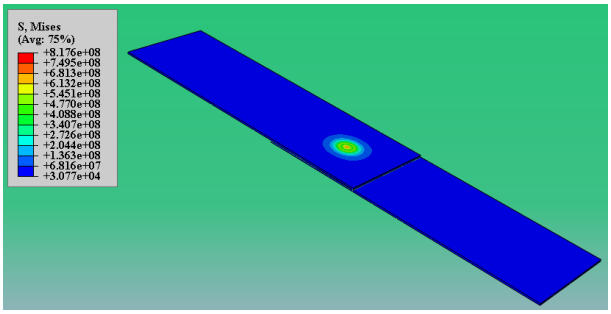

Fig. 7. Von mises stress of the RWS

4. RESULTS AND DISCUSSION

The experimental and numerical investigations yielded critical insights into the resistance spot welding (RSW) behaviour of dissimilar material combinations (37.2 carbon steel, 304 stainless steel, and commercial aluminium).

4.1 Weld Nugget Formation

The growth in weld nuggets with varying currents and welding time revealed material-related phenomena (Fig. 8). For CS-SS joints, diameters grew rapidly from 4.2 mm at 5 kA to 6.2 mm at 9 kA before growth stabilized. This was simultaneous with thermo-equilibrium in the steel-dominating interface where dissipation equalized joule heating—a process previously established in analogous steel combinations [16]. Aluminium-composite joints (CS-Al and SS-Al) registered retarded growth to only 4.8 mm (CS-Al) and 5.1 mm (SS-Al) by 9 kA. This was due to superior conduction (237 W/m·K) in aluminium that dissipated heat from the weld zone, rendering increased currents essential to balance this. Significantly, increased welding time beyond 20 cycles registered minimal diameter increments (<5%), underscoring marginal return to extended heating—of utmost significance to industrial efficiency [35].

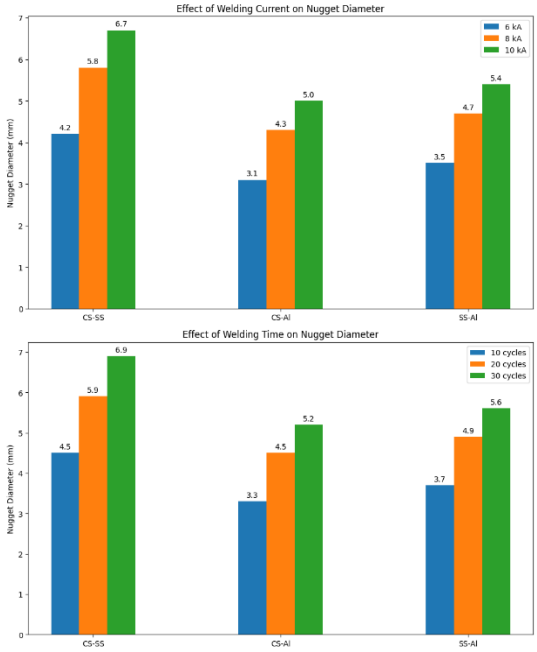

Fig. 8. Nugget diameter vs. welding current and time

4.2 Tensile Shear Strength

Tensile shear performance diverged sharply across material combinations (Fig. 9). CS-SS joints dominated, peaking at 9.5 kN (9 kA)—a strength attributed to metallurgical homogeneity and negligible intermetallic formation. This aligns with Pouranvari [12], who observed analogous trends in steel-steel welds. Conversely, aluminium-steel joints faltered: CS-Al and SS-Al peaked at 3.7 kN (8 kA) and 4.5 kN (8.5 kA), respectively. Post-fracture analysis revealed brittle intermetallic compounds (IMCs) at the steel-aluminium interface, fracturing under load with minimal plasticity—a well-documented Achilles' heel in dissimilar welding [36].

Intriguingly, the relationship between nugget diameter (D*D*) and tensile strength (F) adhered to a power-law model ($F=kD^n$), but exponents diverged: 1.8 (CS-SS), 1.5 (CS-Al), and 1.3 (SS-Al). These exponents act as fingerprints for failure mechanisms: the higher exponent in CS-SS reflects ductile failure in the heat-affected zone (HAZ). At the same time, lower values in Al-steel pairs signal brittle interfacial fracture. Parallel studies on advanced high-strength steels [37] corroborate this trend, though material-specific property variations (e.g., strain hardening in SS-Al) modulate the exponents.

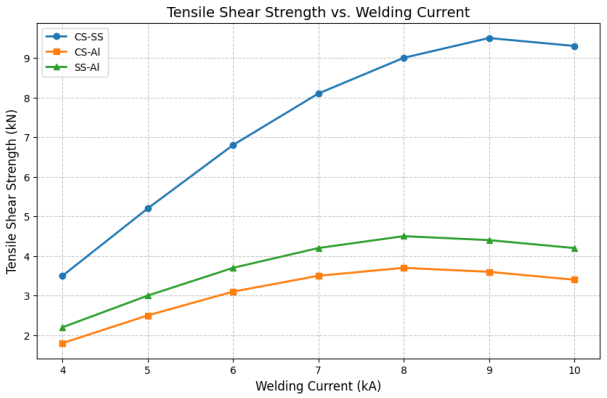

Fig.9. Tensile shear strength vs. welding current for CS-SS, CS-Al, and SS-Al joints

4.3 Stress-Strain Behaviour

The stress-strain curves for the three material combinations exhibited distinct mechanical responses (Fig. 10). Carbon Steel-Stainless Steel (CS-SS) joints demonstrated superior performance, with an ultimate tensile strength (UTS) of approximately 450 MPa and a yield strength of 320 MPa. The extended plastic deformation region (>15% strain) highlighted robust energy absorption capabilities, consistent with ductile failure mechanisms in metallurgically compatible steel pairs [17].

In contrast, Carbon Steel-Aluminium (CS-Al) joints exhibited brittle failure, characterized by a UTS of 220 MPa and minimal plastic deformation (<5% strain). This behaviour was attributed to brittle Fe-Al intermetallic compounds (IMCs) at the weld interface, which facilitated crack propagation under load [36].Stainless Steel-Aluminium (SS-Al) joints displayed intermediate properties, achieving a UTS of 250 MPa and moderate strain hardening before fracture. While stainless steel's strain-hardening capacity improved performance compared to CS-Al, IMC brittleness still limited ductility [38].

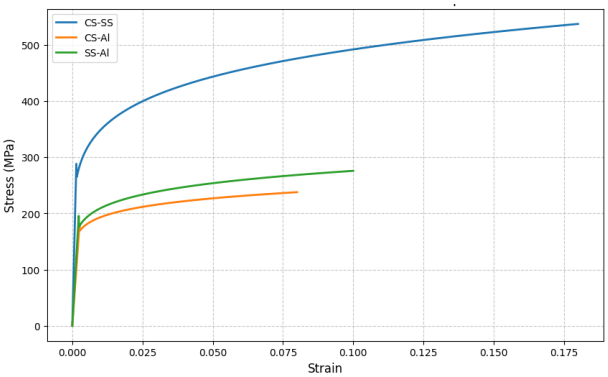

Fig. 10. Stress-strain curves for CS-SS, CS-Al, and SS-Al joints

Key Trends:

- Strength Hierarchy: CS-SS > SS-Al > CS-Al.
- Ductility Ranking: CS-SS > SS-Al > CS-Al.
- Failure Modes:
  - CS-SS: Ductile fracture in the heat-affected zone (HAZ).
  - CS-Al/SS-Al: Brittle interfacial failure dominated by IMCs.

These findings align with prior studies on dissimilar aluminium-steel welds [39] reinforcing the critical role of interfacial reactions in joint performance. The mechanical hierarchy underscores the challenges of balancing strength and ductility in multi-material systems, particularly for automotive applications requiring crash resilience.

4.4 Comparison of Experimental and FEA Results

To validate our computational model and assess its predictive capabilities, we compared our experimental results with predictions from Finite Element Analysis (FEA). Fig. 11a) and b) presents this comparison for nugget diameters and tensile shear strengths across different welding currents and material combinations.

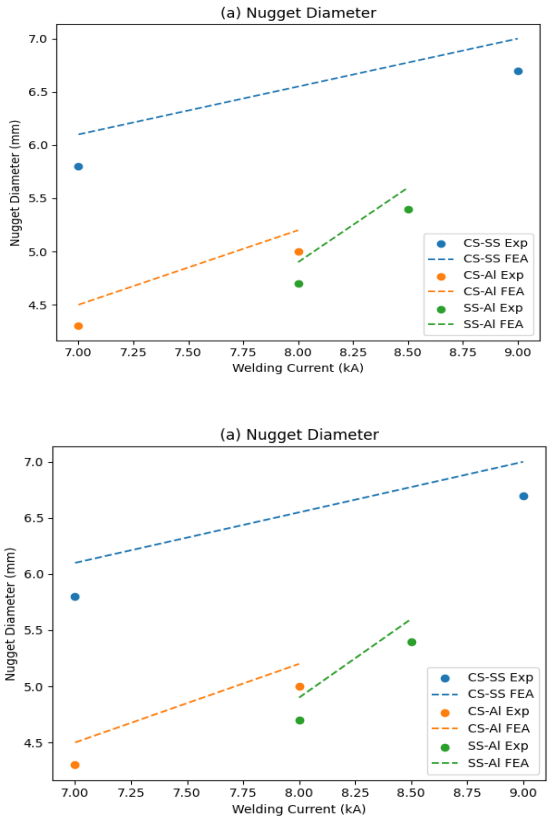

Fig. 11. Comparison of experimental and FEA-predicted results

FEA model agreed well with the experimental results, with average deviations of 7.5% for nugget diameter and 9.2% for tensile shear strength. The model was successful in capturing the trends in nugget growth and strength development for the different welding parameters and material combinations. For nugget diameter predictions, we noted that the FEA model tended to overestimate the size somewhat, particularly for the higher welding currents. This overestimation is perhaps due to the idealized thermal contact conditions in our model, which may not capture the complexities of actual welding interfaces. Kong et al. [13] described similar challenges in their FEA modeling of aluminium alloy spot welds, commenting on the difficulty in accurately representing all the intricacies of the welding process. For the tensile shear strength predictions, our model tended to underestimate the strength for CS-SS joints at the higher currents, while overestimating it somewhat for aluminium-containing joints. These differences are likely due to the challenge in accurately modeling the complex phase transformations and intermetallic compound formation, especially in dissimilar material welds. To further quantify the agreement between our experimental and FEA results, conducted a correlation analysis for nugget diameter and tensile shear strength for all the tested configurations. Fig. 12 presents these correlations.

The correlation for nugget diameter (Fig. 12a) yielded an R^2 value of 0.962, indicating a strong agreement between experimental measurements and FEA predictions. For tensile shear strength (Fig.12 b), it obtained an even higher R^2 value of 0.978. These strong correlations validate our FEA model's ability to predict key weld characteristics across various welding conditions and material combinations. However, it's important to note that we observed more scatter in the CS-SS joint data, particularly for higher strength values. This increased variability could be attributed to the more complex microstructural changes occurring in CS-SS welds, which may be challenging to capture fully in the FEA model. Encountered similar challenges in their modeling of spot welds for crash simulations, emphasizing the ongoing difficulties in accurately representing all aspects of the welding process in computational models [40].

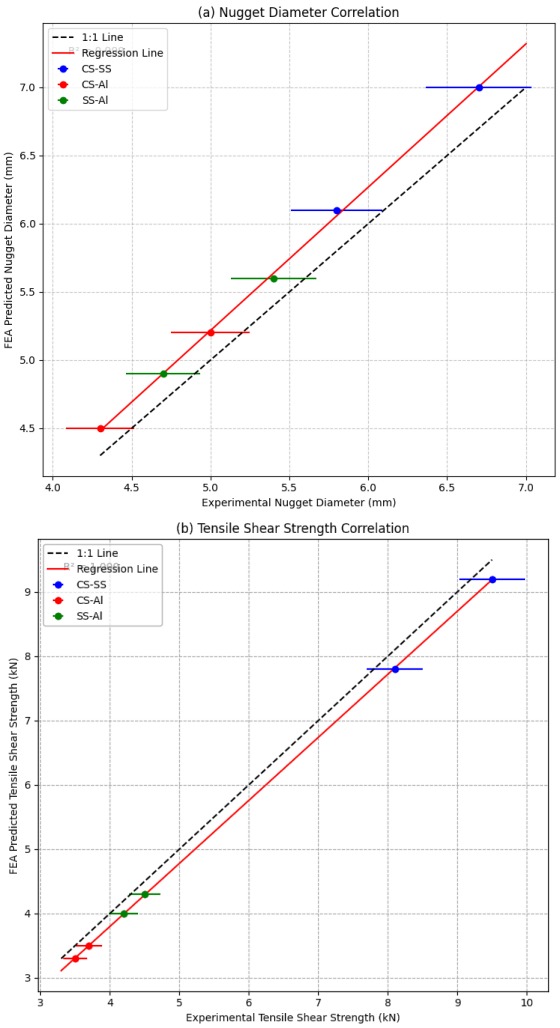

Fig. 12. Correlation between experimental and FEA results

4.5 Comparative Analysis with Literature

To contextualize the findings within the broader field of dissimilar material spot welding, a comparative analysis was conducted with recent literature. The results of this study align closely with prior research while highlighting unique insights into material-specific performance.

The CS-SS joints in this study achieved a peak tensile shear strength of 9.5 kN at 9 kA, with pull-out failures dominating (75% of specimens). These results closely match those reported by [16] who observed 10.2 kN at 10 Ka for low-carbon steel–austenitic stainless-steel joints. The minor difference in strength (5–7%) may stem from variations in base material composition (e.g., carbon content in steel) or sheet thickness [19]. Both studies confirm the superior performance of steel-steel joints due to metallurgical compatibility and minimal intermetallic compound (IMC) formation. For aluminium-containing joints, the

findings show both similarities and differences with prior studies:

- CS-Al Joints: Peak strength of 3.7 kN at 8 kA, with interfacial failures dominating (55% of specimens).
- SS-Al Joints: Peak strength of 4.5 kN at 8.5 kA, showing intermediate ductility and mixed failure modes.

These results align with Sun et al. [38], who reported 4.1 kN at 8.5 kA for DP600 steel–AA5182 aluminium joints, comparable to the SS-Al performance. However, Wan et al. [17] observed slightly lower strength (3.9 kN at 7.5 kA) for Q235 steel–AA6061 aluminium joints, highlighting the influence of alloy composition on weld strength. For instance, AA5182 aluminium's higher magnesium content may enhance interfacial bonding compared to AA6061.

The failure mode distributions in this study are consistent with literature trends:

- CS-SS Joints: Predominantly pull-out failures (75% of specimens), indicating robust weld integrity.
- Aluminium-Steel Joints: Higher incidence of interfacial failures (40–55% of specimens) due to brittle Fe-Al IMCs, as reported in [41].

Zhao et al. [41] observed similar failure mode distributions in aluminium alloy resistance spot welds, reinforcing the critical role of interfacial reactions in joint reliability.

The optimal welding currents for aluminium-steel joints in this study (8–8.5 kA) were slightly higher than literature values reported by [42] This variation could stem from differences in electrode geometry (e.g., tip diameter) or welding machine dynamics (e.g., current stability). Such discrepancies underscore the importance of tailoring parameters to specific material combinations and industrial setups. The consistency in failure modes (pull-out for CS-SS, interfacial for Al-steel) across studies validates the critical role of material compatibility and interfacial reactions in joint performance. Variations in optimal welding currents highlight the need for parameter optimization based on alloy combinations and equipment configurations.

5. CONCLUSION

In this paper, dissimilar material (304 stainless steel, 37.2 carbon steel, and commercial aluminium) resistance spot welding (RSW) was investigated through an integrated experimental and finite element modeling (FEM) technique. Among notable results was that joints between stainless steel and carbon steel (CS-SS) achieved highest tensile shear strength (9.5 kN at 9 kA) owing to metallurgical compatibility whereas joints with aluminium (CS-Al, SS-Al) achieved lower strength owing to intermetallic compounds (IMCs) causing interfacial failures to be brittle in nature, requiring greater current (8–8.5 kA). Hardness differences in welds correlated with failure modes: CS-SR joints with pull-out failures verified superior weld quality whereas interfacial failures in Al-steel combinations revealed continued challenge. Strong prediction ($R^2 > 0.96$) was achieved by the FEM model but required experimental validation to achieve welds with superior strength.

Industrially, CS-SS joints can be used efficiently in aerospace and automotive lightweight structural applications. Friction stir spot welding or adhesive bonding can be employed in Al-steel joints to address limitations in IMCs. Long-term performance (fatigue, corrosion) should be prioritized in future work in addition to interlayer materials to prevent IMCs and advanced FEM models including phase transformations. This work drives RSW optimisation in multi-material constructions to address current-day requirements in engineering.

ACKNOWLEDGMENTS:

The authors thank Mustansiriyah University (College of Engineering) for the use of facilities in their labs.

CONFLICTS OF INTEREST

The authors declare no conflict of interest.

REFERENCES

[1] K. Miyamoto, S. Nakagawa, C. Sugi, H. Sakurai, A. Hirose, Dissimilar joining of aluminum alloy and steel by resistance spot welding. *SAE International Journal of Materials and Manufacturing*, 2(1), 2009: 58–67. https://doi.org/10.4271/2009-01-0034

[2] M. Rashid, S. Fukumoto, J.B. Medley, J. Villafuerte, Y. Zhou, Influence of lubricants on electrode life in resistance spot welding of aluminum alloys. *Welding Journal*, 86, 2007: 62-70.

[3] Y. Yang, Z. Luo, Y. Zhang, J. Su, Dissimilar welding of aluminium to steel: A review. *Journal of Manufacturing Processes*, 110, 2024: 376–397. https://doi.org/10.1016/j.jmapro.2023.12.060

[4] M. Łomozik, A. Hernas, M.L. Zeman, Effect of welding thermal cycles on the structure and properties of simulated heat-affected zone areas in X10CrMoVNb9-1 (T91) steel at a state after 100,000h of operation. *Materials Science and Engineering: A*, 637, 2015: 82–88. https://doi.org/10.1016/j.msea.2015.04.009

[5] J. Dong, J. Hu, Z. Luo, Quality Monitoring of Resistance Spot Welding Based on a Digital Twin. *Metals*, 13(4), 2023: 697. https://doi.org/10.3390/met13040697

[6] K.P. Mehta, V.J. Badheka, A Review on Dissimilar Friction Stir Welding of Copper to Aluminum: Process, Properties, and Variants. *Materials and Manufacturing Processes*, 31(3), 2016: 233–254. https://doi.org/10.1080/10426914.2015.1025971

[7] M. Winnicki, A. Małachowska, M. Korzeniowski, M. Jasiorski, A. Baszczuk, Aluminium to steel resistance spot welding with cold sprayed interlayer. *Surface Engineering*, 34(3), 2018: 235–242. https://doi.org/10.1080/02670844.2016.1271579

[8] K. Mori, Y. Abe, T. Kato, Mechanism of superiority of fatigue strength for aluminium alloy sheets joined by mechanical clinching and self-pierce riveting. *Journal of Materials Processing Technology*, 212(9), 2012: 1900–1905. https://doi.org/10.1016/j.jmatprotec.2012.04.017

[9] L. Shi, J. Xue, J. Kang, A.S. Haselhuhn, H. Ghassemi-Armaki, B.E. Carlson, Fatigue behavior of three-sheet aluminum-steel dissimilar resistance spot welds for automotive applications. *Procedia Structural Integrity*, 51, 2023: 102–108. https://doi.org/10.1016/j.prostr.2023.10.074

[10] J. Liu, G. Xu, X. Gu, G. Zhou, Ultrasonic test of resistance spot welds based on wavelet package analysis. *Ultrasonics*, 56, 2015: 557–565. https://doi.org/10.1016/j.ultras.2014.10.013

[11] R. Verma, K.S. Arora, L. Sharma, R. Chhibber, Experimental investigation on resistance spot welding of dissimilar weld joints. *Proceedings of the Institution of Mechanical Engineers, Part E: Journal of Process Mechanical Engineering*, 235(2), 2020: 505–513. https://doi.org/10.1177/0954408920968351

[12] M. Pouranvari, Critical assessment 27: Dissimilar resistance spot welding of aluminium/steel: Challenges and opportunities. Materials Science and Technology, 33(15), 2017: 1705–1712. https://doi.org/10.1080/02670836.2017.1334310

[13] X. Kong, Q. Yang, B. Li, G. Rothwell, R. English, X.J. Ren, Numerical study of strengths of spot-welded joints of steel. Materials & Design, 29(8), 2008: 1554–1561. https://doi.org/10.1016/j.matdes.2007.12.001

[14] A.S. Adkine, S.K. Biradar, A review of the effects of resistance spot welding on metallurgical and mechanical characteristics. *Welding International*, 39(2), 2025: 52–65. https://doi.org/10.1080/09507116.2024.2419551

[15] P. Russo Spena, M. De Maddis, F. Lombardi, M. Rossini, Investigation on resistance spot welding of TWIP steel sheets. *Steel Research International*, 86(12), 2015: 1480–1489. https://doi.org/10.1002/srin.201400336

[16] M. Pouranvari, S.P.H. Marashi, Critical review of automotive steels spot welding: process, structure and properties. *Science and Technology of Welding and Joining*, 18(5), 2013: 361–403. https://doi.org/10.1179/1362171813Y.0000000120

[17] Z. Wan, H.-P. Wang, N. Chen, M. Wang, B.E. Carlson, Characterization of intermetallic compound at the interfaces of Al-steel resistance spot welds. *Journal of Materials Processing Technology,* 242, 2017: 12–23. https://doi.org/10.1016/j.jmatprotec.2016.11.017

[18] H. Zhang, J. Senkara, X. Wu, Suppressing cracking in resistance welding AA5754 by mechanical means. Journal of Manufacturing Science and Engineering, 124(1), 2002: 79–85. https://doi.org/10.1115/1.1418693

[19] S.K. Khanna, X. Long, 4 - Fatigue behavior of spot welded joints in steel sheets. In: X. Sun (ed.), *Failure Mechanisms of Advanced Welding Processes. Woodhead Publishing*, 2010: 65–100. https://doi.org/10.1533/9781845699765.65

[20] L. Bogaerts, A. Dejans, M.G.R. Faes, D. Moens, A machine learning approach for efficient and robust resistance spot welding monitoring. *Welding in the World*, 67, 2023: 1923–1935. https://doi.org/10.1007/s40194-023-01519-1

[21] S. Shin, D.-J. Park, J. Yu, S. Rhee, Resistance Spot Welding of Aluminum Alloy and Carbon

Steel with Spooling Process Tapes. *Metals*, 9(4), 2019: 410. https://doi.org/10.3390/met9040410

[22] Y. Zhao, W. Wang, X. Wei, Optimization of Resistance Spot Welding with Inserted Strips via FEM and Response Surface Methodology. *Materials*, 14(23), 2021: 7489. https://doi.org/10.3390/ma14237489

[23] T. Matsukage, S. Sakurai, T. Traui, M. Iyota, Mechanical Properties of Resistance-Spot-Welded Joints of Aluminum Castings and Wrought Alloys. Engineering Proceedings, 43(1), 2023: 52. https://doi.org/10.3390/engproc2023043052

[24] A.A.F. Ogaili, K.A. Mohammed, A.A. Jaber, A.E.S. Al, Automated wind turbines gearbox condition monitoring: A comparative study of machine learning techniques based on vibration analysis. *FME Transactions*, 52(3), 2024: 471–485. https://doi.org/10.5937/fme2403471O

[25] K.A. Mohammed, M.N.M. Al-Sabbagh, A.A.F. Ogaili, E.S. Al-Ameen, Experimental analysis of hot machining parameters in surface finishing of crankshaft. *Journal of Mechanical Engineering Research and Developments*, 43(4), 2020: 105–114.

[26] A.A.F. Ogaili, M.N. Hamzah, A.A. Jaber, Enhanced Fault Detection of Wind Turbine Using eXtreme Gradient Boosting Technique Based on Nonstationary Vibration Analysis. *Journal of Failure Analysis and Prevention*, 24, 2024: 877-895. https://doi.org/10.1007/s11668-024-01894-x

[27] S.A. Al-Haddad, M.Y. Fattah, T.K. Al-Azawi, L.A. Al-Haddad, Three-dimensional analysis of steel beam-column bolted connections. Open Engineering, 14(1), 2024: 20220579. https://doi.org/10.1515/eng-2022-0579

[28] M.Y. Fattah, L.A. Al-Haddad, M. Ayasrah, A.A. Jaber, S.A. Al-Haddad, Coupled Finite Element and Artificial Neural Network Analysis of Interfering Strip Footings in Saturated Cohesive Soils. Transportation Infrastructure Geotechnology, 11, 2024: 2168-2185. https://doi.org/10.1007/s40515-023-00369-0

[29] L.A. Al-Haddad, L. Ibraheem, A.I. EL-Seesy, A.A. Jaber, S.A. Al-Haddad, R. Khosrozadeh, Thermal Heat Flux Distribution Prediction in an Electrical Vehicle Battery Cell Using Finite Element Analysis and Neural Network. Green Energy and Intelligent Transportation, 3(3), 2024: 100155. https://doi.org/10.1016/j.geits.2024.100155

[30] A.A.F. Ogaili, Q.S. Mahdi, E.S. Al-Ameen, A.A. Jaber, E.K. Njim, Finite-element investigations on the influence of material selection and geometrical parameters on dental implant performance. *Curved and Layered Structures,* 11(1), 2024: 20240015. https://doi.org/10.1515/cls-2024-0015

[31] Y. Wang, Z. Rao, F. Wang, Heat evolution and nugget formation of resistance spot welding under multi-pulsed current waveforms. *The International Journal of Advanced Manufacturing Technology*, 111, 2020: 3583–3595. https://doi.org/10.1007/s00170-020-06337-z

[32] A.A.F. Ogaili, M.N. Hamzah, A.A. Jaber, Free Vibration Analysis of a Wind Turbine Blade Made of Composite Materials. *17th International Middle Eastern Simulation and Modelling Conference - MESM 2022*, 27 June 2022, Baghdad, Iraq, pp.203–209.

[33] P. Chigurupati, B.K. Chun, A. Bandar, W.T. Wu, Finite Element Modeling of Resistance Spot Welding Process. *International Journal of Material Forming*, 3, 2010: 991–994. https://doi.org/10.1007/s12289-010-0936-4

[34] H. Huang, H. Murakawa, A Selective Integration-Based Adaptive Mesh Refinement Approach for Accurate and Efficient Welding Process Simulation. *Journal of Manufacturing and Materials Processing*, 7(6), 2023: 206. https://doi.org/10.3390/jmmp7060206

[35] X. Sun, E.V. Stephens, M.A. Khaleel, H. Shao, M. Kimchi, Resistance Spot Welding of Aluminum Alloy to Steel with Transition Material — From Process to Performance — Part I: Experimental Study. *Welding Journal*, 2004: 188-195.

[36] O.S. Barrak, S. Ben-Elechi, S. Chatti, Parameters influence on mechanical properties of resistance spot welding: AISI304L/AISI1005. *Pollack Periodica*, 2024. https://doi.org/10.1556/606.2024.01142

[37] V.H. Baltazar Hernandez, S.K. Panda, Y. Okita, N.Y. Zhou, A study on heat affected zone softening in resistance spot welded dual phase steel by nanoindentation. *Journal of Materials Science*, 45, 2010: 1638–1647. https://doi.org/10.1007/s10853-009-4141-0

[38] M. Sun, S.T. Niknejad, H. Gao, L. Wu, Y. Zhou, Mechanical properties of dissimilar resistance spot welds of aluminum to magnesium with Sn-coated steel interlayer. *Materials & Design*, 91, 2016: 331–339. https://doi.org/10.1016/j.matdes.2015.11.121

[39] M. Ghosh, K. Kumar, R.S. Mishra, Analysis of microstructural evolution during friction stir welding of ultrahigh-strength steel. *Scripta Materialia,* 63(8), 2010: 851–854. https://doi.org/10.1016/j.scriptamat.2010.06.032

[40] A.A.F. Ogaili, A. AbdulhadyJaber, M.N. Hamzah, Statistically Optimal Vibration Feature Selection for Fault Diagnosis in Wind Turbine Blade. *International Journal of Renewable Energy Research*, 13(3), 2023: 1082–1092. https://doi.org/10.20508/ijrer.v13i3.14096.g8782

[41] D.W. Zhao, Y.X. Wang, L. Zhang, P. Zhang, Effects of electrode force on microstructure and mechanical behavior of the resistance spot welded DP600 joint. *Materials & Design*, 50, 2013: 72–77. https://doi.org/10.1016/j.matdes.2013.02.016

[42] M.M. Hamzah, O.S. Barrak, I.T. Abdullah, A.A. Hussein, S.K. Hussein, Process Parameters Influence the Mechanical Properties and Nugget Diameter of AISI 316 Stainless Steel During Resistance Spot Welding. *International Journal of Applied Mechanics and Engineering*, 29(2), 2024: 79–89. https://doi.org/10.59441/ijame/186956